

Frost growth parameters in a forced air stream

R. ÖSTIN and S. ANDERSSON

Department of Applied Physics, University of Umeå, Sweden

(Received 10 January 1989 and in final form 16 June 1990)

Abstract—The formation of frost on parallel horizontal plates facing a forced air stream is studied at varying temperatures, relative humidities and air velocities. Both the surface temperature of the plates and the relative humidity of the air stream are found to have important effects for the frost thickness. The density of frost is found to increase with relative humidity and especially air velocity. A dynamic one strip method is applied to determine the thermal conductivity, which is used in order to study internal changes in the frost layer. Two categories of frost formation are observed—monotonic and cyclic growth. In the former it is found that the condensed water vapour contributes in equal amounts to increases in the thickness and the density while in the latter melting at the frost surface results in abrupt internal densification.

1. INTRODUCTION

WHEN A humid air stream is brought in contact with a cooled surface at a temperature below the dew and the freezing temperatures, condensation and frosting will occur on the surface. This is a well-known fact in processes where heat is transferred to a refrigerated surface as in air-to-air heat exchangers.

This paper will report on frost formation in the plate-type non-storing heat exchanger, which recovers sensible heat only if frosting does not occur as a result of the cool air stream. A serious problem in a cold climate is that frost and furthermore ice will form on the exhaust channel walls of the exchanger. This reduces the efficiency and may result in damage by expansion of the ice.

The long-term aim of our investigation is to study the possibility of decreasing the frost formation by applying low adhesive hydrophobic surface coatings. As a preliminary to this, the present work reports on an investigation of frost formation on uncoated surfaces. An experimental apparatus has been built to simulate the conditions in a counter flow heat exchanger. The first part of the work has been to obtain information on frost formation by observing the dependence on plate surface temperature, relative humidity and air velocity. A study of the frost, developed under different environmental conditions, was performed by considering density and thermal conductivity.

2. EXPERIMENTAL APPARATUS

As the aim has been to study frosting in the air-to-air heat exchanger we attempted to simulate conditions which would arise in practice but a certain degree of simplification was necessary in order to perform the experiment. In the experimental setup there was only one air stream and that was the warm air stream. The presence of the cold air was simulated by

a set of cooling coils and heating elements attached to the plates. The regulation of the heaters was handled by a computer program based on the assumption that both the warm and the fictitious cold air flow had an equal energy content which is a special case in the theory of counter flow heat exchangers. This simplifies the temperature distribution to a linear function of distance from the entrance edge and along the plates.

The experimental apparatus is shown in Fig. 1. The air was forced to circle in a closed loop of pipes made from transparent polyvinyl chloride. The loop was connected to a climate chamber in which flow, humidity and temperature of the air were controlled. The moisture content of the air was controlled by a humidifier which used a plate of quartz vibrating at high frequency. The relative humidity was recorded by means of a commercially available probe (VAISALA HMP 112Y) which used a capacitive principle of measurement and which had a maximum error of $\pm 5\%$.

Before the air entered the space between the cold plates it was forced through a honeycomb to produce a fully-developed flow. The entrance was made of plates of aluminium which were glued together using a flexible silicone adhesive. This construction made the two cooling plates mobile and different cross-section areas of the air channel could thereby be obtained. The actual area of testing (see Fig. 2) was on the two aluminium plates which were each 10 mm thick, 800 mm long and 300 mm wide. The sides of the cooling plates were supported by Plexiglas which made it possible to visually observe the development of frost.

In order to achieve a linear surface temperature distribution electrical surface heaters and cooling coils were attached to the plate on the side opposite to the surface which faced the air flow. Plate temperatures were measured by chromel vs alumel thermocouples mounted in a row of drilled holes evenly spaced along the centreline of the cooling plates. The depth of the

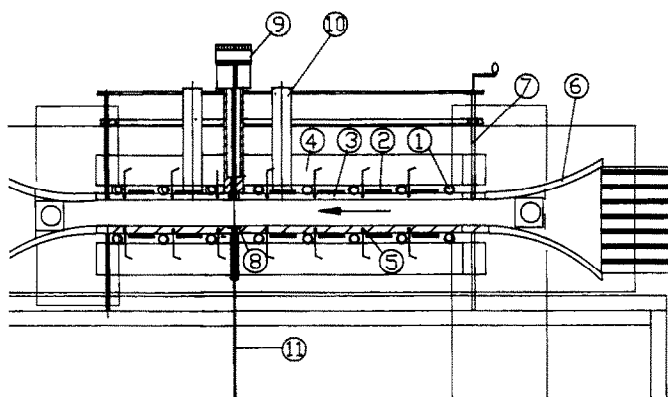


FIG. 2. Illustration of the actual area of testing: 1, cooling coils; 2, surface heaters; 3, aluminium plates; 4, insulation; 5, thermocouples; 6, entrance; 7, mechanism for changing the cross-sectional area between the plates; 8, cavity for the weighing plate; 9, micrometer; 10, lead-through for the micrometer; 11, shaft attached to the weighing plate.

computer which was serial interfaced to a HP 3497A data acquisition system.

3.2. Frost thickness

The thickness of frost was measured by a micrometer with a resolution of 0.005 mm. A reading was taken when the shaft of the micrometer touched the frost surface. To ensure reproducibility of measurement, the end of the micrometer shaft was observed visually using a fibre optic endoscope with illumination from the opposite side of the shaft. The criterion for reading was when there was no light between the end of the shaft and the frost surface. The error in the measurement was estimated as ± 0.1 mm. A thickness value was determined by taking the average of four measurements at different locations around the area of weighing.

3.3. Mass and density

The mass of the frost deposit was recorded by a digital weighing machine (Mettler PE 3600). A cavity of area $25 \times 80 \text{ mm}^2$ and 5 mm in depth was formed at a distance of 595 mm from the entrance on the lower heat exchanger plate. A weighing plate of aluminium with a shaft attached to it was machined to fit this cavity (see Fig. 2). By changing the distance between the cold plates the shaft was brought in contact with the weighing machine. The advantage of the method was that weighing could be done repeatedly in its original environment. A problem to overcome was the friction between the shaft and the bearing at the lead-through of the cold plate. The friction was decreased by using bearings of lapped bakelite and a clearance of 0.1 mm in the bearing. The error in the weighing was estimated as 0.07 g (7×10^{-5} kg). The mass and thickness measurements gave an average

density without any information about gradients in the frost layer.

3.4. Velocity

The flow rate was measured by a pitot tube connected to a differential pressure transducer. The pitot tube was placed in a straight tube between conical sections. The error given by the manufacturer was $\pm 1\%$ for the pitot tube and the error for the actual setup was estimated as $\pm 5\%$. The wind velocity in the area was calculated by the continuity equation for incompressible steady flow.

3.5. Thermal conductivity

Previous workers [1, 2] have analysed energy transport in frost layers under conditions similar to those of our experiments. Following these workers, we assume that energy transport is due mainly to solid-state conduction in the frost structure and to diffusion of water vapour. An effective thermal conductivity K , including conduction and mass diffusion, is defined by

$$K = \lambda_c + \lambda_d \quad (1)$$

where λ_c is the solid-state conduction contribution and λ_d the conduction due to diffusion of water vapour.

According to ref. [3] the energy equation is given by

$$\rho c_p \frac{\partial T}{\partial t} = \nabla \cdot (K \nabla T) \quad (2)$$

where

$$K = \lambda_c + i_{\text{fg}} \beta_o(T). \quad (3)$$

Equation (2) was derived by assuming that the frost

was isotropic and homogeneous, that the water vapour diffusion was caused by pressure gradients and that Clapeyron's equation could be applied.

In order to measure the thermal properties, K and ρc_p (heat capacity per unit volume), of the growing frost layer, we decided to apply the transient one-strip method [4]. Advantages of the method are that neither the frost surface temperature nor the heat transferred through the frost layer need to be measured. Based on equation (2) we used as an approximation the solution to the case of pure conduction in isotropic and homogeneous media with the thermal properties independent of temperature and position.

3.6. Method of measurement

In the transient one-strip method a constant heating power is supplied to the specimen during a finite time by means of a heater strip which is in good thermal contact with the specimen. Using the heater strip as a resistance thermometer the temperature rise due to the supplied heating power is recorded vs time. By fitting the appropriate theoretical expression to the measured temperature rise of the strip, typically 2–3 K, the thermal properties λ and ρc_p of the specimen may be extracted.

In the thermal measurements a thin strip of Pt foil, $0.013 \times 48 \times 0.45$ mm, was glued to the surface of a plate, $2 \times 60 \times 18$ mm, of poly(methyl methacrylate), PMMA. The PMMA with the attached Pt strip, which will hereafter be referred to as the probe, was then positioned in a cavity in the weighing plate described in Section 3.3. The measurements were then performed on the frost layer growing on the probe surface.

With knowledge of λ and ρc_p of one medium, i.e. the probe material, the corresponding properties of the frost may be obtained by fitting equation (A1) (see Appendix) to experimental data. In our case the thermal properties of the probe material were determined separately as a function of temperature by measurements in vacuum. For the PMMA probes which were used we obtained $\lambda = 0.20 \text{ W m}^{-1} \text{ K}^{-1}$ and $\rho c_p = 1.49 \text{ MJ m}^{-3} \text{ K}^{-1}$ at 273 K. The values of c_p which were calculated from ρc_p were within 2% from the c_p values obtained with a differential scanning calorimeter. In the analysis of the measured temperature rise of the strip the effect of the heat capacity of the Pt strip was taken into account in terms of a time lag at the onset of the heater power [5].

With the present two-media technique, uncertainty in the input data of λ and ρc_p of the probe affects the accuracy of the measured values of λ and ρc_p of the specimen. To minimize this influence the ratio of $\lambda \cdot \rho c_p$ (specimen) to $\lambda \cdot \rho c_p$ (probe) would ideally be very high and thereby give a high value of σ (see Appendix). A high value of σ means that most of the heat supplied to the strip goes into the specimen. However, when using a probe material (Styrofoam HI30-E) with a very low thermal conductivity $\lambda = 0.03$, compared to $\lambda = 0.20 \text{ W m}^{-1} \text{ K}^{-1}$ for

Table 1. Temperature, relative humidity and calculated values of mass flux of condensed vapour for the different test runs. The air velocity was the same (3 m s^{-1}) for all the runs. Figures within parentheses are the variation in the variable during the test

Run No.	T_{ai} [°C]	T_p [°C]	RH_{ai} [%]	$J_f \times 10^{-5}$ [$\text{kg m}^{-2} \text{ s}^{-1}$]
1	20.5(0.6)	-7.0(0.2)	32.2(1.6)	3.67
2	20.6(0.7)	-6.9(0.2)	52.0(2.3)	8.14
3	20.6(0.7)	-6.5(0.2)	75.1(3.9)	15.10
4	21.1(1.4)	-10.8(0.2)	31.1(6.6)	4.21
5	20.6(0.7)	-10.7(0.2)	51.4(4.5)	10.60
6	20.5(0.6)	-10.7(0.2)	72.0(6.4)	14.40
7	20.9(1.2)	-19.9(0.2)	33.3(4.9)	5.82
8	20.8(1.1)	-19.6(0.2)	54.5(5.8)	12.60
9	20.3(0.6)	-19.7(0.2)	73.6(6.3)	19.00

PMMA, we found that a practical problem arose in that frost formation was very limited. An additional consideration is that the probe material must also not absorb water vapour, which did occur for WACKER WDS (SiO_2 65.4%, FeO 14.8%, TiO_2 16.3%, Al_2O_3 2.3%, B_2O_3 0.5% and 0.7% sulphate and chloride). In our experiments we found that PMMA was a good compromise as probe material.

4. RESULTS AND DISCUSSION

This experimental study was performed at the different environmental conditions compiled in Table 1. The results which were obtained could be classified into two categories.

(1) Test runs where the frost thickness increases as shown by Fig. 3 with a best fit according to

$$\delta = a_0 + a_1 \sqrt{t} \quad (4)$$

which is in agreement with what others [3, 6–8] have found.

(2) Test runs with a cyclic increase in frost thickness, as described by Fig. 4, with a significant increase in

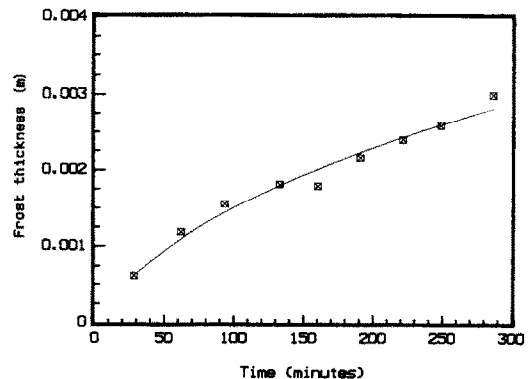


FIG. 3. Typical result showing monotonic growth of frost; variation of frost thickness with time.

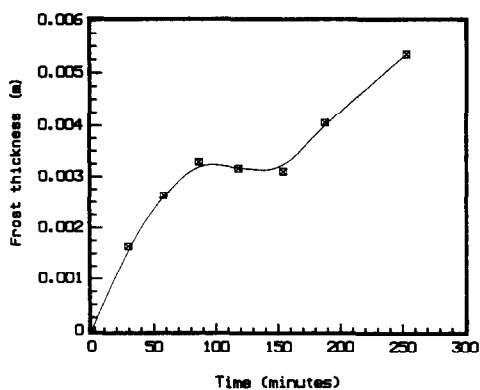


FIG. 4. Typical result showing cyclic growth of frost; variation of frost thickness with time.

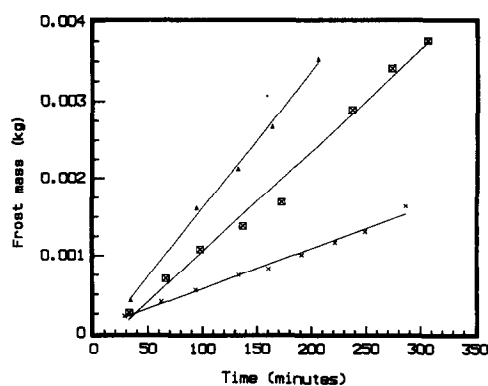


FIG. 6. Frost mass vs time at different RH of inlet air: x, run No. 4; □, run No. 5; △, run No. 6.

the density. This category will be discussed further in Section 4.4 below.

4.1. Frost mass, thickness and density

The frost mass was found to increase linearly with time for different plate temperatures and air humidities. The rate of increase of frost mass with time (mass rate) was found to be almost independent of the cold plate temperature (Fig. 5), whereas the inlet air humidity had a more pronounced effect (Fig. 6). The mass rate increased by a factor of 2.3 and 3.6 at 51 and 72% humidity, respectively, compared with the 31% test run. The small dependence of the mass rate on the cold plate temperature shows an insulating effect from the frost layer. Once frost has developed on the plate and the frost surface temperature has risen to a constant value, after the initial transient period of frost formation [9], further frost deposition is mainly dependent on the air humidity.

Both the cold plate temperature and the air humidity were found to have a large effect on the frost thickness. From Fig. 7 one notices that a decrease of the cold plate temperature from -7 to -20°C almost doubled (99%) the frost thickness for an inlet air humidity of 30%. When increasing the inlet air humidity from 31 to 72% (Fig. 8) at a cold plate

temperature of -10°C the frost thickness increased by 86%. The same tendency has been reported in refs. [6, 10] over a smaller range of humidity. These results combined with the results on the deposited frost mass shows that low surface temperatures result in a frost layer of low density while increase of the humidity results in frost layers with high density. The highest density values in this study were obtained in test runs No. 2 and No. 3 (Table 1) and were in the range $400\text{--}680\text{ kg m}^{-3}$.

During the time of frost formation, both thickness and density of frost were found to increase. In order to study the partitioning of the condensed vapour between these two variables, the conservation of mass concept was used. Starting with the mass of frost expressed as

$$m_f = A\rho\delta \tag{5}$$

and taking the partial derivatives with respect to time we obtain

$$\frac{\delta \cdot \partial \rho}{\partial t} + \frac{\rho \cdot \partial \delta}{\partial t} = \frac{1}{A} \frac{\partial m_f}{\partial t} = J_f \tag{6}$$

which may be written as

$$m_p + m_\delta = J_f \tag{7}$$

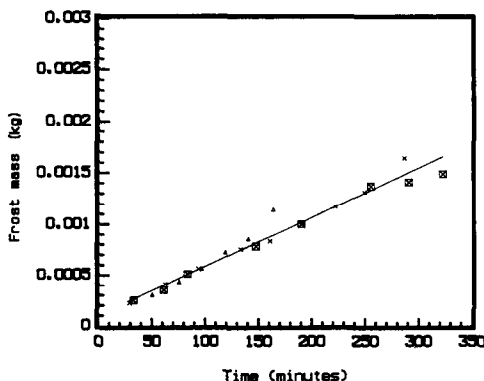


FIG. 5. Frost mass vs time at different cold plate temperatures: □, run No. 1; x, run No. 4, △, run No. 7.

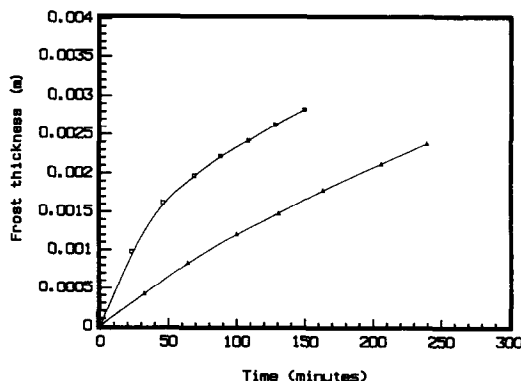


FIG. 7. Frost thickness vs time at different cold plate temperatures: △, run No. 1; □, run No. 7.

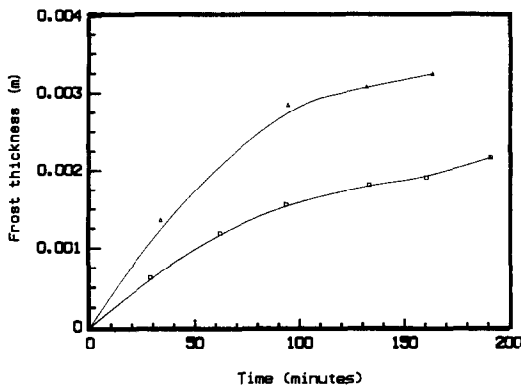


FIG. 8. Frost thickness vs time at different RH of inlet air: □, run No. 4; △, run No. 6.

where J_f is the mass flux of condensed vapour from the air stream to the frost, and m_p and m_s are the parts of J_f which add to the frost density and thickness, respectively. The ratio m_s/J_f , calculated from our experimental values of m_f and ρ , was found to vary between 0.41 and 0.65 with an average value of 0.49. Values close to the average were obtained at times greater than 60 min, compared with the first recorded values which were typically obtained at 25 min. Our results for m_s/J_f indicate that half of the condensed water vapour increased the thickness and the other half increased the density of the frost layer, which is in agreement with the hypothesis of ref. [3].

The effect of air velocity on the thickness was found to be negligible which is in agreement with the results of other investigators [6, 8, 10]. Our study of the effect of air velocity was for a Reynolds number in the range 6.130–13.440. We did not detect a thickness dependence at Reynolds numbers lower than 15.900 as was reported in ref. [11]. The effect of velocity on the mass rate was considerable. The mass rate increased by a factor of 2.4 for a test run with a velocity of 5.7 m s^{-1} compared to 2.6 m s^{-1} . The effect on the frost density is shown in Fig. 9. It can be

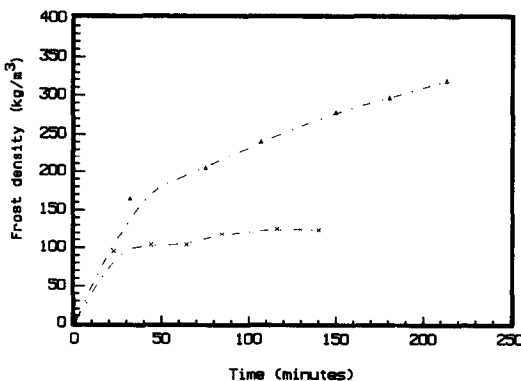


FIG. 9. Frost density vs time at different air velocities: ×, 2.6 m s^{-1} ; △, 5.7 m s^{-1} . RH and T_p were 32% and -15.3°C , respectively, during the test runs.

seen that the density increases both in absolute values and in rate with the higher air velocity. Compiling our experimental results from the study of the effects from cold plate temperature, relative humidity and air velocity on frost we conclude that changing the plate temperature mainly affects the frost thickness, changing the relative humidity affects both frost thickness and mass rate, changing the air velocity mainly affects the mass rate of frost.

4.2. Comparison with models

Since our experimental results were mainly for times greater than 1 h a quasi-stationary model was chosen for comparison with the experimental values. Our results were in agreement, within experimental accuracy, with the simple model of ref. [3], in which frost thickness and density are related by

$$\frac{\rho}{\rho_o} = \frac{\delta}{\delta_o} = \sqrt{1 + \tau}$$

where

$$\tau = \frac{m_o(t - t_o)}{\rho_o \delta_o} \quad (8)$$

ρ_o , δ_o and m_o are the frost density, thickness and mass at time t_o . The time t_o is when quasi-stationary conditions have been reached, i.e. when the heat flux through the frost layer and the frost surface temperature have become constant.

Independent verification that the quasi-stationary condition has been established would require continuous measurements of heat flux through the layer and the surface temperature but this would have been impractical. What we did, as a test for the establishment of the quasi-stationary condition, was to deduce an average value of t_o from: (a) the time at which a linear increase of thermal conductivity values with thickness of the frost was detected, and (b) the time from which m_s/J_f was approximately equal to 1/2 (cf. equation (7)). When this value of t_o and the corresponding values of ρ_o , δ_o and m_o were substituted in equation (8) we found that agreement with experiment was within $\pm 10\%$.

A number of more or less complex models have been reported in the literature [8, 12, 13] but use of these typically requires knowledge or estimation of a substantial number of physical parameters. In view of the good agreement we have found with the simple model of ref. [3], we conclude that use of these more complex models would not be justified.

4.3. Thermal conductivity of frost

The values of the measured effective thermal conductivity from all the test runs in Table 1 are shown in Fig. 10. Our experimental data were described within experimental inaccuracy by the polynomial

$$\lambda = -8.71 \times 10^{-3} + 4.39 \times 10^{-4} \rho + 1.05 \times 10^{-6} \rho^2 \quad (9)$$

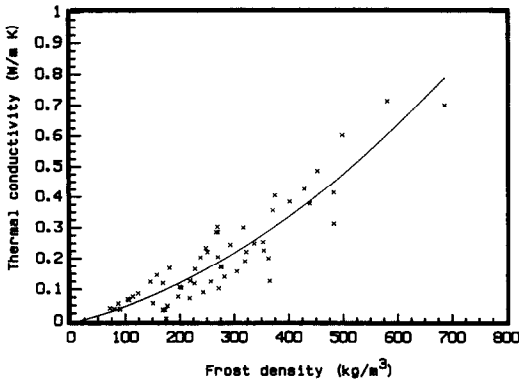


FIG. 10. Effective thermal conductivity of frost vs frost density.

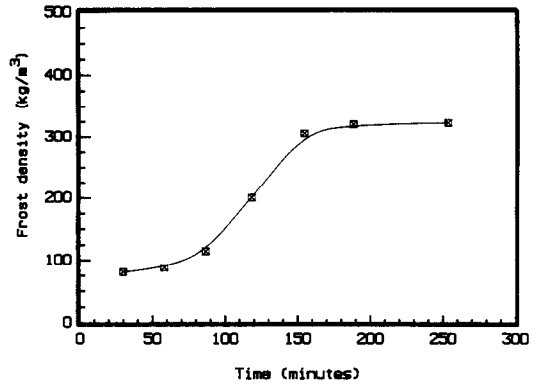


FIG. 12. Typical frost density vs time for cyclic frost growth.

Our experimental results for the effective thermal conductivity are somewhat lower than the results of other workers [6, 14–17]. Compared to the average values of those investigations our values are within a factor of 1.31 lower in the density range 100–550 kg m⁻³. A good agreement of our values for the effective thermal conductivity was found with the values of ref. [17]. In the density range 100–550 kg m⁻³ the agreement was within a factor of 1.04. Compiling the results from the previous investigations one finds a rather broad scatter in the relation between thermal conductivity and density. This scatter could be explained by errors in the methods of measurement, especially in the technique to determine the density, and by differences in the experimental conditions.

After the initial period of the early stages of frost formation has passed the thermal conductivity should depend linearly on thickness according to Fourier's law. This has been used as the criterion that a quasi-stationary condition was reached in order to determine t_0 in Section 4.1. Typical results from test runs No. 1 and No. 7 are shown in Fig. 11. From the figure the result of run No. 1 indicated that the condition was reached after 150 min while the results of run No. 7 indicated the condition to be reached after 50 min.

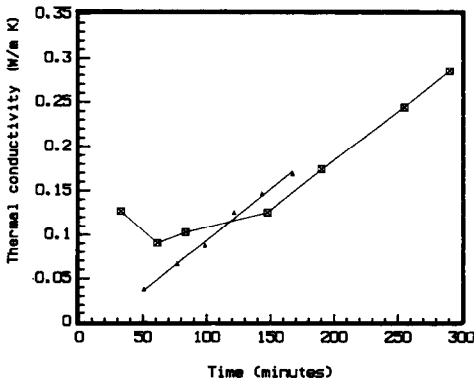


FIG. 11. Typical results showing effective thermal conductivity of frost vs frost thickness: \square , run No. 1; \triangle , run No. 7.

Our results for the heat capacity per unit volume, ρc_p , were about ten times higher than what was expected from taking c_p of frost equal to c_p of ice. A test of the one-strip method, when the specimen was solid ice, showed a discrepancy of 10% in both λ and ρc_p compared with literature values [18]. The values of ρc_p were found to decrease somewhat with increasing frost density. The temperature rise of the strip and the heating time were varied but no effect on the values of ρc_p was noticed. When the frost on the probe was compressed manually the measured values of ρc_p decreased to less than twice that of ice. The reason for our high measured values of ρc_p of frost is unclear. One explanation could be that sublimation or evaporation takes place in the porous frost structure at the interface of the frost and the strip. If so, then the experimental values of ρc_p would be expected to decrease with increasing density when manually compressing the frost on the probe.

4.4. Abrupt densification of the frost layer

The category two results (cyclic increase in frost thickness) were characterized by a frost thickness vs time plot like that shown in Figs. 12 and 13, respectively. The density can be seen to increase by a factor

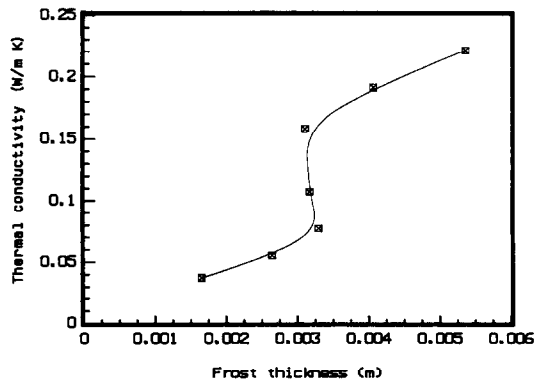


FIG. 13. Typical effective thermal conductivity of frost vs frost thickness in the cyclic frost growth case.

of 3. From the thermal conductivity vs thickness (Fig. 13) one can observe a linear increase in the conductivity and a stepwise increase by a factor of 2 at the thickness value corresponding to the plateau in Fig. 4. Thereafter the conductivity again increases as observed initially. The same abrupt densification process has been observed in other test runs under conditions that the air stream humidity was $\geq 50\%$ and the plate surface temperature was $\leq -10^\circ\text{C}$. Whatever the detailed nature of the densification process, we conclude that it must affect the frost layer down to close to the substrate since otherwise the measured thermal conductivity would be relatively unchanged. Although we did not visually observe water droplets on the frost surface there is a further piece of evidence which suggests that melting at the frost surface was the reason for the cyclic increase of the thickness and the abrupt increase of the density. This is that it was noticed that the frost surface was rough and uneven after the first hour of testing while at the end of these tests the frost surface looked smooth. Melting at the frost surface has been reported by other workers. In refs. [19, 20] melting was described as a cyclic process of water film formation, water permeation, freezing and further frosting. The melting process was found to be triggered by the frost surface temperature reaching 0°C as a result of increasing frost thermal resistance with increasing frost thickness.

5. SUMMARY

Frost formation was studied in an experimental apparatus simulating the conditions in a counter flow air heat exchanger. Two categories of formation were observed, monotonic growth and cyclic growth. The latter was interpreted as due to melting at the frost surface. For the monotonic growth, thickness and density were found to increase in agreement with the model of ref. [3], with the condensed water vapour from the forced air stream contributing in equal amounts to increases in the thickness and the density. This indicates that the frost formation process takes place both on the surface and inside the frost layer.

A dynamic one strip method was used in order to measure the frost thermal conductivity, K . Our results for the variation of conductivity with density agreed with previous investigations. We found somewhat high values for ρc_p (heat capacity per unit volume), which could be due to sublimation or evaporation of water. However, we consider our experimental values of thermal conductivity to give a good description of $K(\rho, \delta)$.

In cases where melting at the frost surface was suggested to have occurred the thermal conductivity values indicated that water drained through the whole frost layer. At the same time, there was a large and abrupt increase in density and a slight decrease in thickness of the frost layer. We conclude that when

abrupt internal densification takes place it is due to melting at the frost surface.

The cold plate temperature and the relative humidity were found to have important effects for the enhancement of frost thickness while thickness was found to be negligible of air velocity. However, the velocity influenced the frost layer internally as the density was found to increase with higher velocities.

Acknowledgement—This work was financially supported by the National Swedish Board for Technical Development.

REFERENCES

1. H. Auracher, Effective thermal conductivity of frost, *Heat Mass Transfer Refrig.* **24**, 285–302 (1987).
2. M. A. Dietenberger, Generalized correlation of water frost thermal conductivity, *Int. J. Heat Mass Transfer* **26**, 607–619 (1983).
3. J. E. White, Heat and mass transfer in thick frost layers, Ph.D. Thesis, Engineering Heat, University of Kentucky (1973).
4. S. Gustafsson and E. Karawacki, Transient hot-strip probe for measuring thermal properties of insulating solids and liquids, *Rev. Scient. Instrum.* **54**(6), 744–747 (1983).
5. S. Andersson, Determination of thermophysical properties under hydrostatic pressure, Ph.D. Thesis, Department of Physics, University of Umeå (1988).
6. J. D. Yonko and C. F. Sepsy, An investigation of the thermal conductivity of frost while forming on a flat horizontal plate, Preprint No. 2043, ASHRAE 74th Annual Meeting, Minneapolis (1967).
7. K. Aoki, M. Hattori and T. Itoh, A study of extended surface heat exchangers with frosting, *Bull. JSME* **29**(251), 1499–1505 (1986).
8. H. W. Schneider, Equation of growth rate of frost forming on cooled surfaces, *Int. J. Heat Mass Transfer* **21**, 1019–1024 (1978).
9. P. L. T. Brian, R. C. Reid and I. Brazinsky, Cryogenic frost properties, *Cryogenic Technol.* **5**, 205–212 (1969).
10. N. Seki, S. Fukusako and K. Matsuo, An analysis of incipient frost formation, *Bull. JSME* **27**(233), 2476–2482 (1984).
11. D. L. O'Neal, The effect of frost formation on the performance of a parallel plate heat exchanger, Ph.D. Thesis, Purdue University (1982).
12. B. W. Jones and J. D. Parker, Frost formation with varying environmental parameters, *J. Heat Transfer, Trans. ASME* **97**, 255–259 (1975).
13. A. A. Rostami, Condensation and frost formation in heat exchangers, Ph.D. Thesis, Department of Mechanical Engineering, University of California, Berkeley (1982).
14. Data attributed by ref. [6] to H. Abels, *Rep. Meteor.* **16**(1) (1983).
15. J. Devaux, Radiothermic economy of fields of snow and glaciers, *Science Abstr., Serie A* **36**, 980–981 (1933).
16. A. S. Kondrat'eva, Thermal conductivity of snow cover and physical process caused by the temperature gradients, S.I.P.R.E. Translation No. 22 (1954).
17. H. Lotz, Wärme und Staffaustauschvorgänge in bereifenden Lammellenrippen Luftkühlern im Zusammenhang mit deren Betriebsverhalten., Technischen Hochschule Aschen (1968).
18. P. V. Hobbs, *Ice Physics*. Oxford University Press, London (1974).
19. G. I. Trammel, J. Canterbury and E. M. Killgore, Heat transfer from humid air to a horizontal flat plate held at sub-freezing temperatures, *ASHRAE Trans.* **73**(2024), Part I, IV.3.1–IV.3.6 (1967).

20. K. Aoki, A study on frost formation (the process of frost formation involving the phenomena of water permeation and freezing), *Bull. JSME* 26(211), 87–93 (1983).
21. O. Nilsson, dc-ac hot-wire procedure for determining thermophysical properties under pressure, *Rev. Scient. Instrum.* 57(9), 2303–2309 (1986).
22. S. Andersson and G. Bäckström, Techniques for determining thermal conductivity and heat capacity under hydrostatic pressure, *Rev. Scient. Instrum.* 57(8), 1633–1639 (1986).
23. H. S. Carslaw and J. C. Jaeger, *Conduction of Heat in Solids*, pp. 375–376. Oxford University Press, London (1959).

APPENDIX

The electronics used to measure the thermal properties of the frost are described in ref. [21]. In general terms a constant heating power was established by supplying d.c. current to the Pt strip. The temperature rise due to this heating was determined with a bridge circuit using a weak superimposed a.c. current and locking technique.

The theoretical expression for the temperature rise in the case of heating and temperature sensing at the interface between two media [21] was derived from the solution to an instantaneous point source of unit strength [22]. The temperature rise at a point $(x, y, 0)$, due to an infinite strip, $-w < x < w$ (strip width) and length $-\infty < y < \infty$ with a negligible heat capacity continuously supplied with a constant heating power q per unit length, is then given by

$$\Delta T = \frac{qa_1\sigma}{w\lambda_1(\sigma^2-1)} \left(\frac{t}{4\pi a_1} \right)^{1/2} \left[F_2 - \frac{F_1}{\sigma} + (I_+ - I_-) \right] \quad (\text{A1})$$

where

$$F_j = \operatorname{erf} z_{j+} - \operatorname{erf} z_{j-} + \frac{1}{\sqrt{\pi}} [z_{j+} + E_1(z_{j+}^2) - z_{j-} - E_1(z_{j-}^2)] \quad (\text{A2})$$

$$I_{\pm} = \frac{1}{2\sqrt{\pi}} \int_{z_{\pm}^2}^{z_{\pm}^2 +} \frac{E_1(y) dy}{\left[(1-s)y + \frac{s(x \pm w)^2}{4a_2 t} \right]^{1/2}}$$

$$z_{j-} = \frac{x \pm w}{(4a_1 t)^{1/2}}; \quad s = \frac{(\sigma^2 - 1)}{(k^2 - 1)};$$

$$k = \sqrt{\left(\frac{a_2}{a_1} \right)}; \quad \sigma = \left(\frac{\lambda_2 \rho_2 c_{p2}}{\lambda_1 \rho_1 c_{p1}} \right)^{1/2}$$

$$a_j = \frac{\lambda_j}{\rho_j c_{pj}} \quad (\text{A3})$$

where

$$K = \lambda_2; \quad \rho c_{pf} = \rho_2 c_{p2}$$

λ_1 and $\rho_1 c_{p1}$ denote thermal properties of the probe.

Equation (A1) is an alternative expression of equation (6) in ref. [21]. For purposes of fitting the experimental data, equation (A1) was averaged over the strip width by numerical integration.

PARAMETRES DE CROISSANCE DU GIVRE DANS UN ECOULEMENT D'AIR FORCE

Résumé—On étudie la formation du givre sur des plaques parallèles horizontales faisant face à un courant d'air, pour des températures, des humidités relatives et des vitesses d'air différentes. La température de la surface ainsi que l'humidité relative de l'air ont des effets importants sur l'épaisseur du givre. La densité du givre augmente avec l'humidité relative et spécialement avec la vitesse de l'air. Une méthode dynamique à une bande est appliquée pour déterminer la conductivité thermique qui est utilisée de façon à étudier les changements internes dans la couche de givre. On observe deux catégories de formation de givre, la croissance monotone et celle cyclique. Dans la première la vapeur d'eau condensée contribue de façon égale à l'accroissement d'épaisseur et de densité tandis que dans l'autre la fusion à la surface du givre cause une densification interne abrupte.

PARAMETER FÜR DIE REIFBILDUNG IN EINEM LUFTSTROM

Zusammenfassung—Die Bildung von Reif auf parallelen, horizontalen Platten, die einem Luftstrom ausgesetzt sind, wird für verschiedene Temperaturen, relative Luftfeuchtigkeiten und -geschwindigkeiten untersucht. Sowohl die Oberflächentemperatur der Platten als auch die relative Feuchtigkeit des Luftstroms üben einen wichtigen Einfluß auf die Dicke der Reifschicht aus. Die Dichte des Reifs nimmt mit der relativen Feuchtigkeit und insbesondere mit der Luftgeschwindigkeit zu. Eine dynamische Einstreifenmethode wird angewandt, um die Wärmeleitfähigkeit zu bestimmen, mit deren Hilfe innere Veränderungen in der Reifschicht untersucht werden. Zwei verschiedene Arten der Reifbildung werden beobachtet: Monotones und zyklisches Wachstum. Im ersten Fall zeigt sich, daß der kondensierte Wasserdampf gleichmäßig zum Wachsen der Schichtdicke und der Dichte beiträgt, während im zweiten Fall ein Schmelzen an der Reifoberfläche zu einer abrupten inneren Verdichtung führt.

ПАРАМЕТРЫ СЛОЯ ИНЕЯ, ОБРАЗУЮЩЕГОСЯ ПРИ ВЫНУЖДЕННОМ ТЕЧЕНИИ ВОЗДУХА

Аннотация—Исследуется образование инея на параллельных горизонтальных пластинах, стоящих на пути вынужденного потока воздуха, при изменяющихся температуре, относительной влажности и скорости воздуха. Найденно, что как температура поверхности пластины, так и относительная влажность потока воздуха оказывают значительное влияние на толщину слоя инея. Обнаружено, что плотность инея увеличивается с ростом относительной влажности и в особенности скорости воздуха. Для определения теплопроводности слоя инея применяется динамический однополосный метод. Наблюдаются два типа процесса образования инея—монотонный и циклический рост. В первом случае найдено, что конденсированный водяной пар в одинаковой степени влияет на увеличение толщины и плотности, в то время как во втором случае таяние инея на поверхности приводит к внезапному внутреннему уплотнению.